Supplement of Biogeosciences, 22, 2225–2238, 2025
https://doi.org/10.5194/bg-22-2225-2025-supplement

Biogeosciences Open Access EGU

Supplement of

Ecosystem leaf area, gross primary production, and evapotranspiration responses to wildfire in the Columbia River basin

Mingjie Shi et al.

Correspondence to: Mingjie Shi (mingjie.shi@pnnl.gov)

Figures.

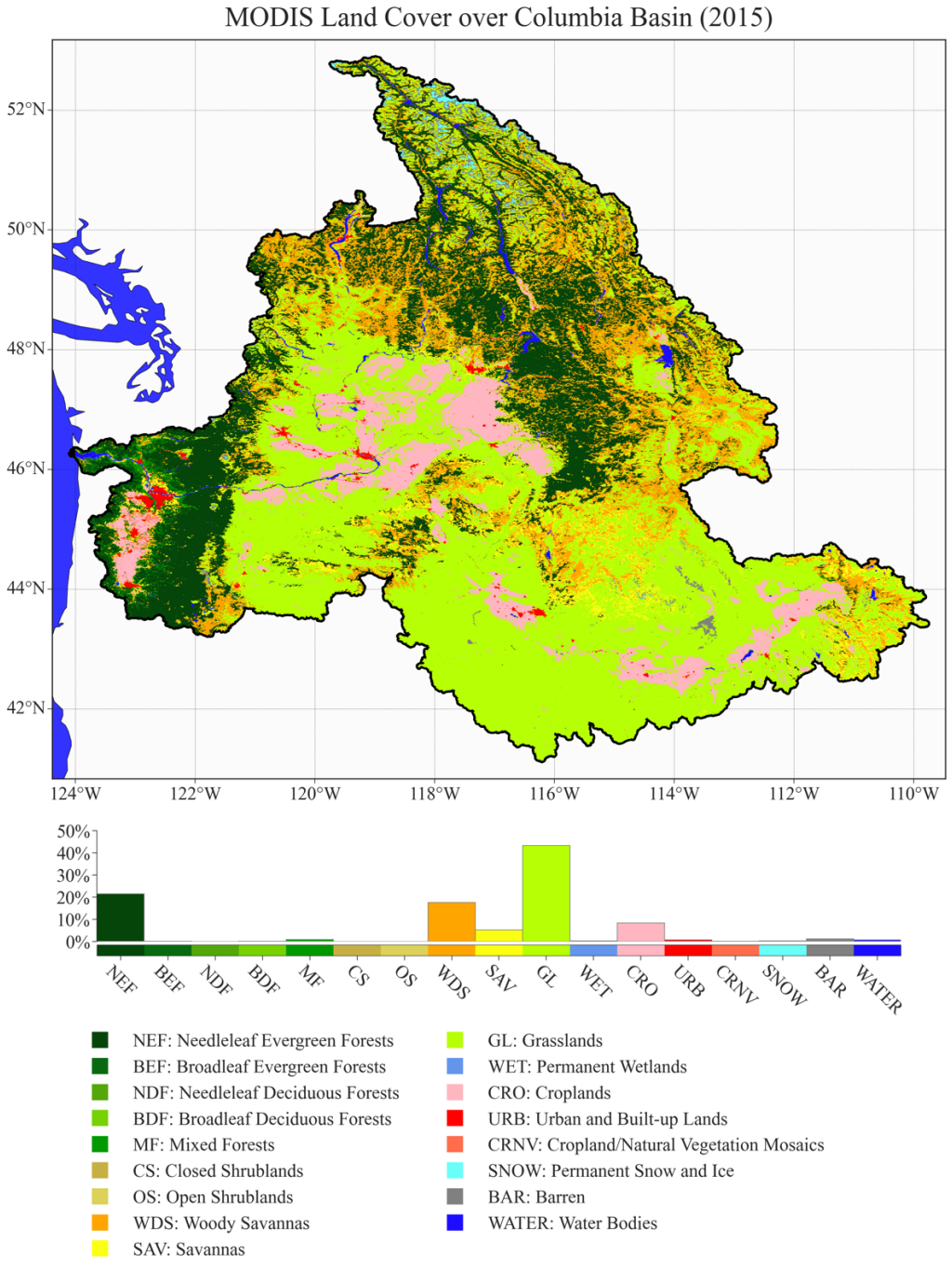

Figure S1. The MODIS MCD12Q1 land cover type (LCT) in 2015.

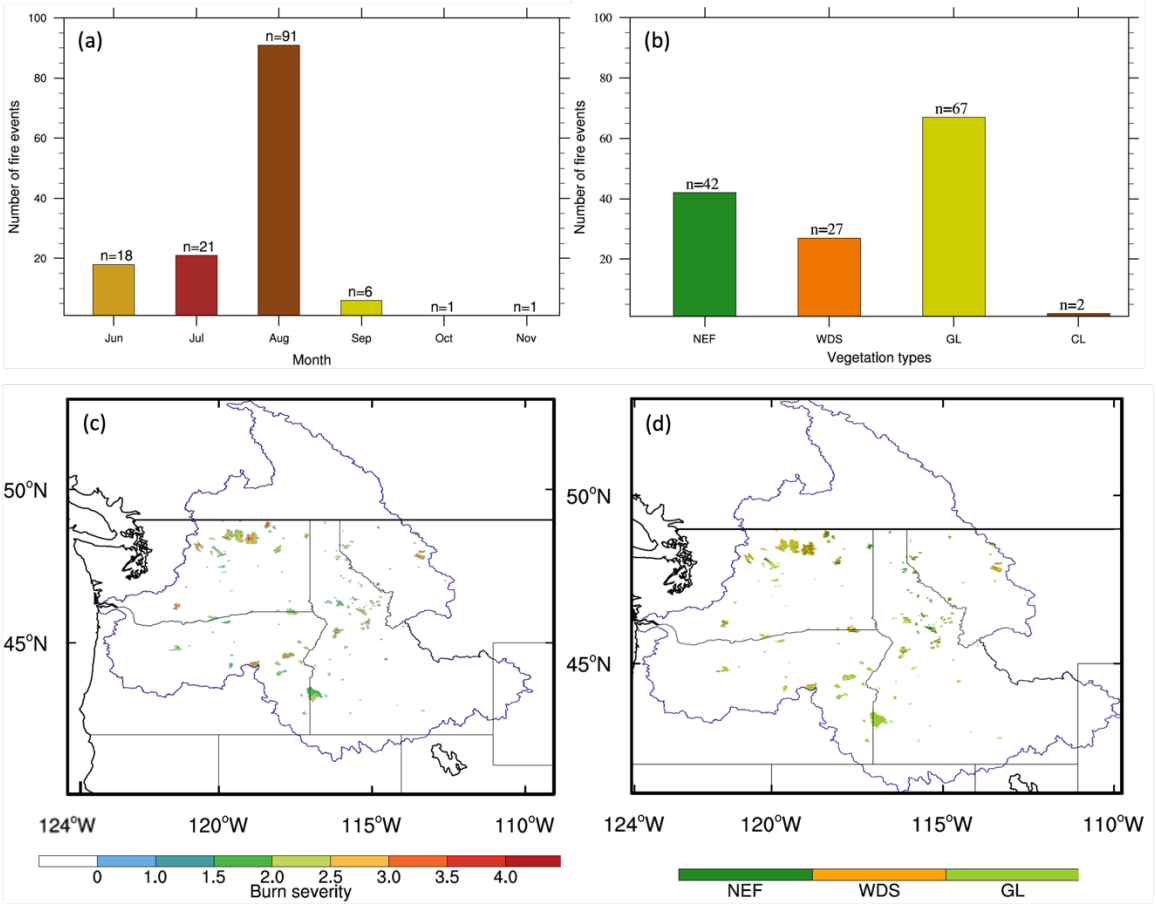

Figure S2. (a) The MTBS data suggested numbers of fire events during June–November, and (b) the number of fire events characterized by the dominant vegetation types (VTs) in each fire boundary, where the VT information is from the MODIS land cover type (LCT). The total number of fire events is 138 in the Columbia River basin in 2015, and their spatial distribution is in (c). The fire boundaries in (c) are applied to Figure 1 to obtain (d), which shows the VT of each burnt data pixel. NEF, WDS, GL, and CL represent needleleaf evergreen forest, woody savanna, grassland, and cropland, respectively.

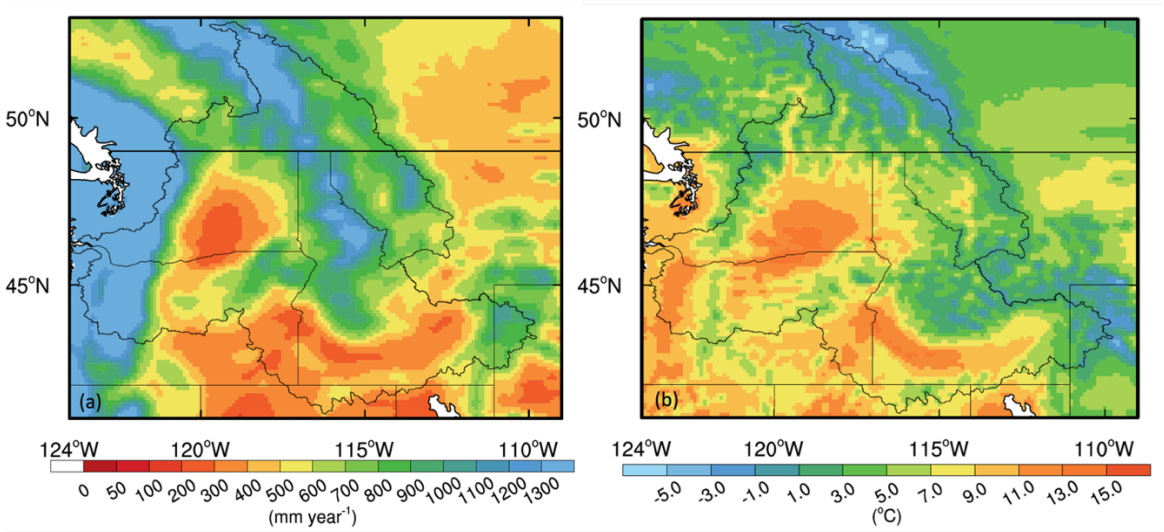

Figure S3. ERA5 suggested climatological (2011–2020) (a) precipitation and (b) surface air temperature over the Columbia River basin.

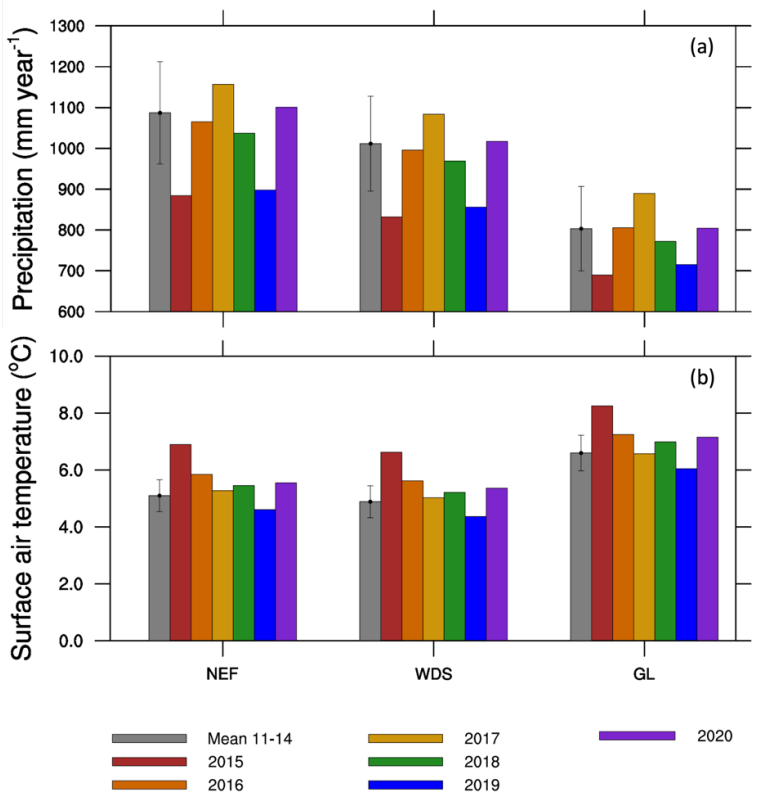

Figure S4. Mean annual (a) precipitation and (b) surface air temperature within the burned sites of the three different vegetation types. NEF: needleleaf evergreen forests, WDS:

woody savannas, and GL: grasslands. The gray bars represent the pre-fire mean values from 2011 to 2014.

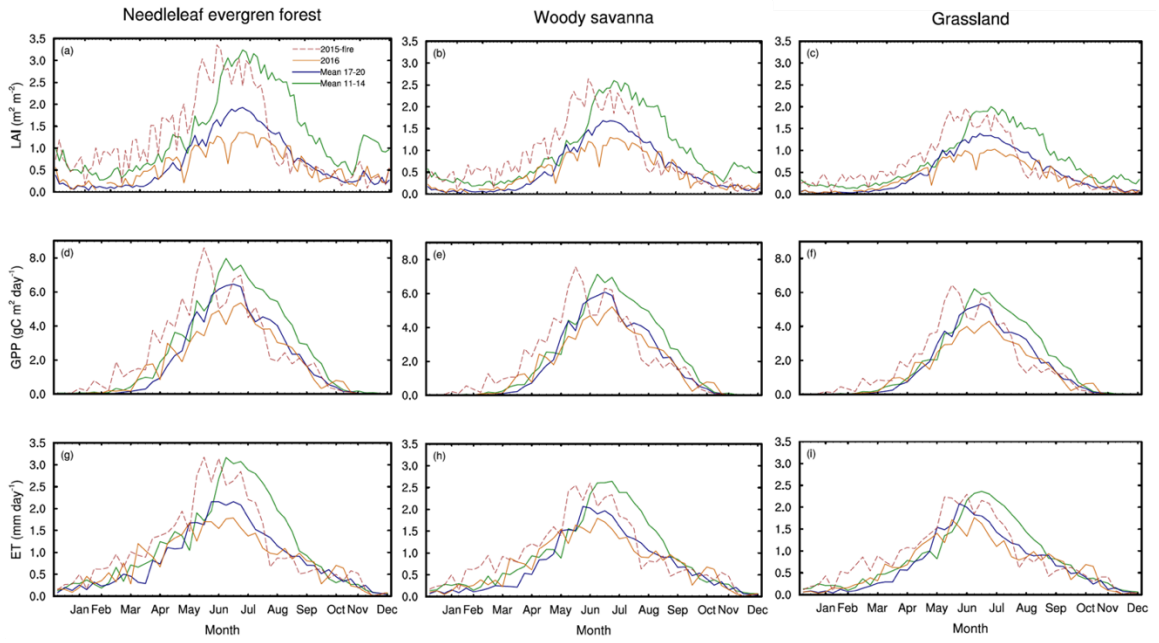

Figure S5. The LAI, GPP, and ET seasonality in 2011–2014 mean, 2015, 2016, and 2017–2020 mean for the needleleaf evergreen forest, woody savanna, and grassland ecosystems with burn severity larger than 3.

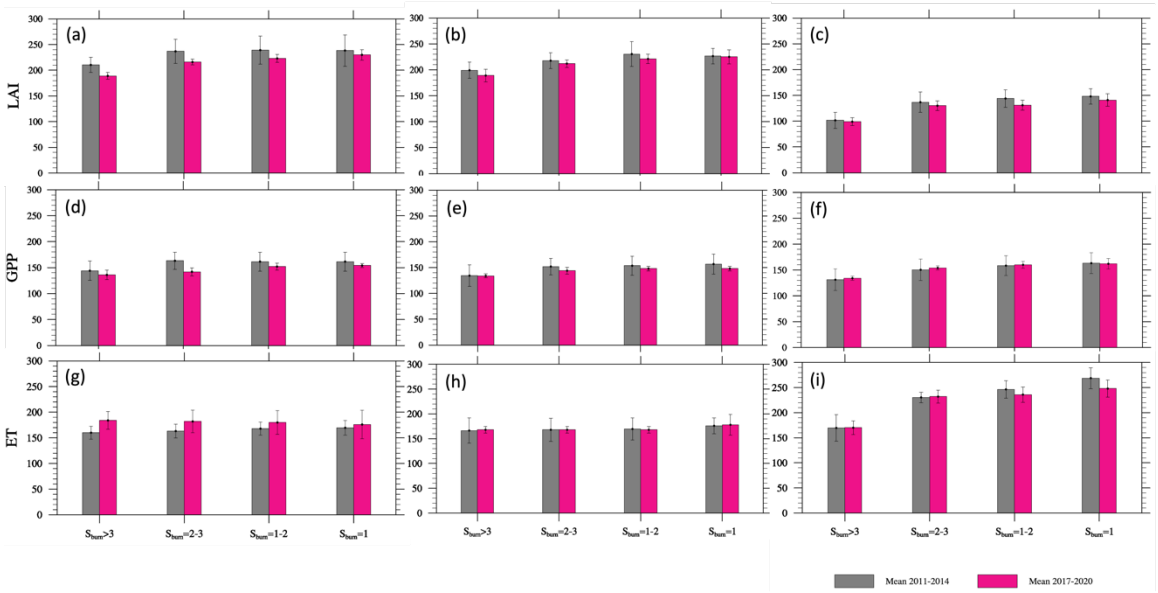

Figure S6. LAI estimated growing season length for (a) NEF, (b) WDS, and (c) GL LCTs; GPP estimated growing season length for (d) NEF, (d) WDS, and (f) GL LCTs; ET estimated growing season length for (g) NEF, (h) WDS, and (i) GL LCTs. The mean values during 2011–2014 and during 2017–2020 are included.

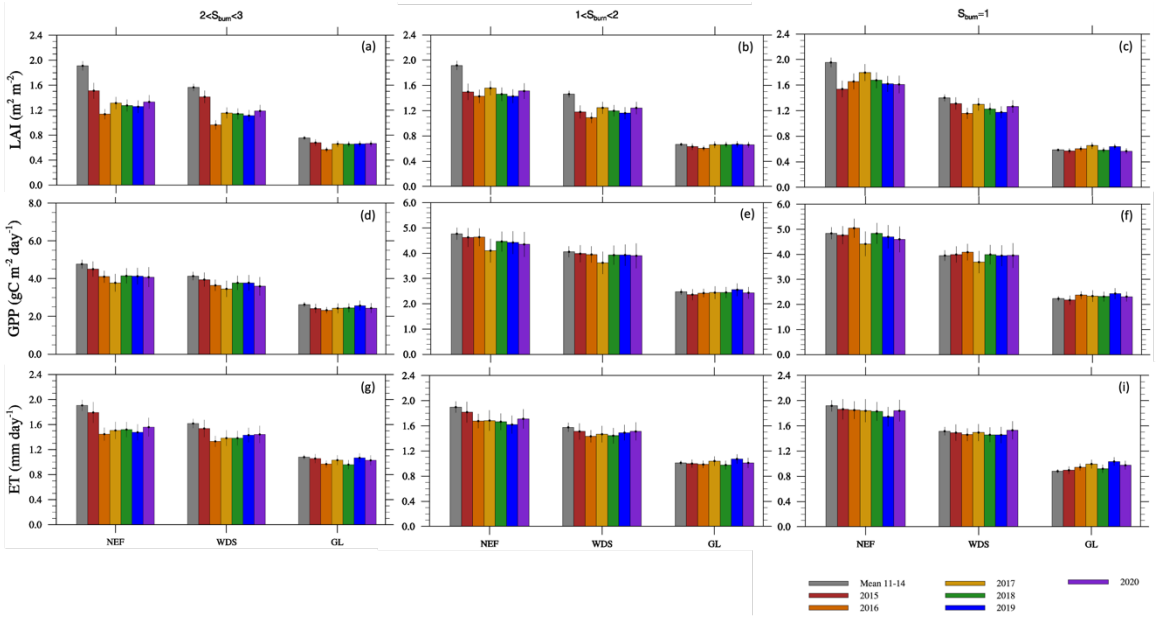

Figure S7. The growing season MODIS LAI with burn severity ranges (a) 2–3, (b) 1–2, and (c) equal to 1; the growing season MODIS GPP with burn severity ranges (d) 2–3, (e) 1–2, and (f) equal to 1; the growing season MODIS Et with burn severity ranges (g) 2–3, (h) 1–2, and (i) equal to 1. The standard errors are included on the bars to represent the data variability across data pixels of different VTs.

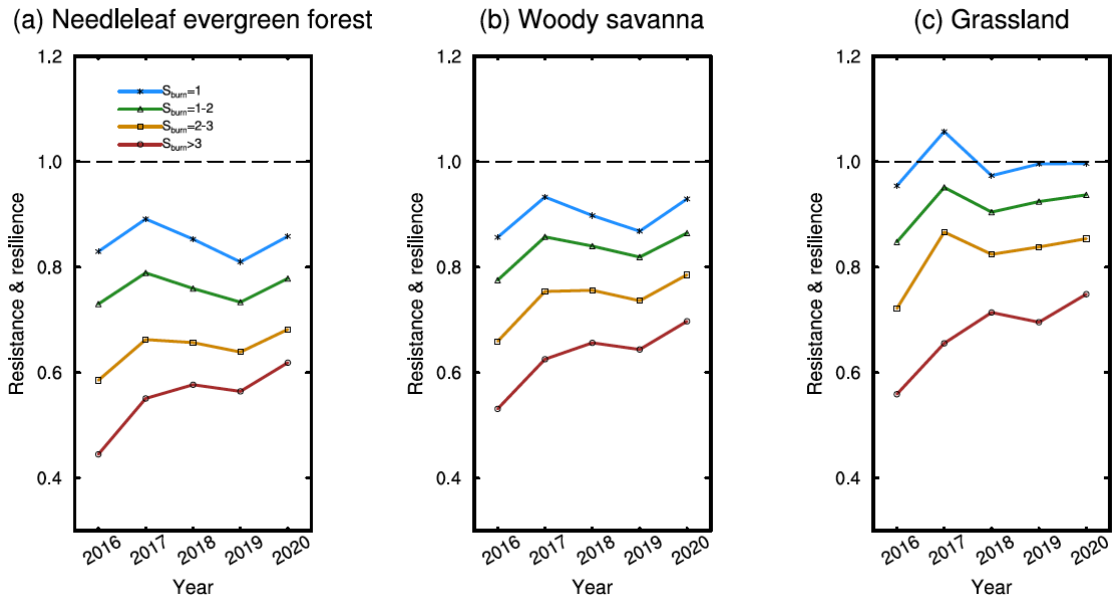

Figure S8. LAI characterized temporal trends in fire resistance (2016) and resilience (years 2017–2020) for (a) needleleaf evergreen, (b) woody savanna, and (c) grassland with four burn severity categories.

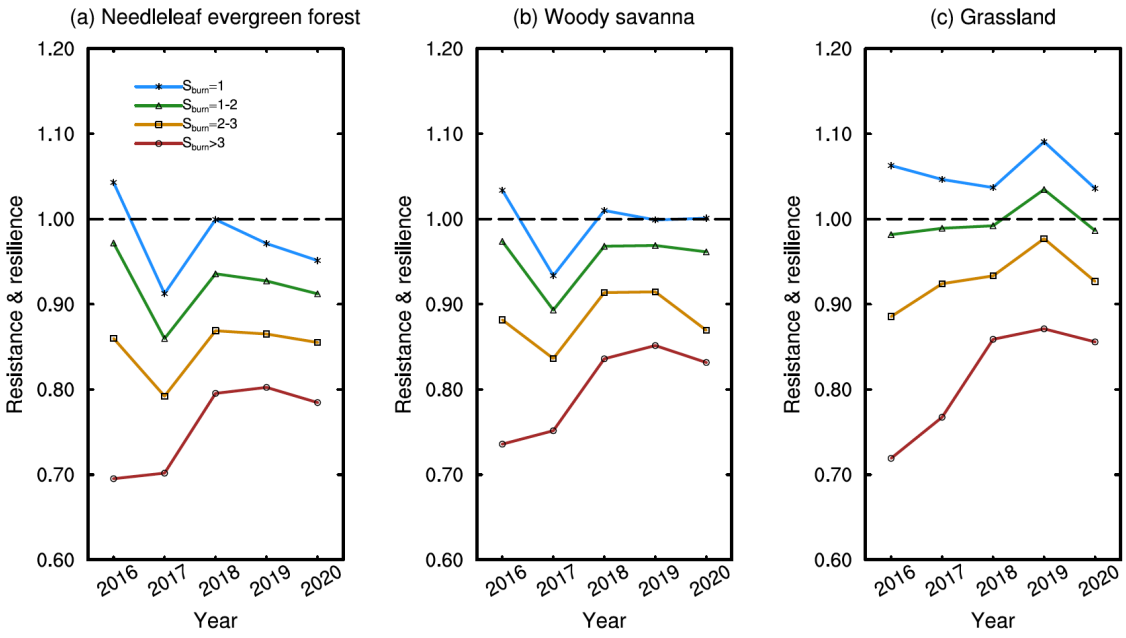

Figure S9. GPP characterized temporal trends in fire resistance (2016) and resilience (2017–2020) for (a) needleleaf evergreen, (b) woody savanna, and (c) grassland with four burn severity categories.

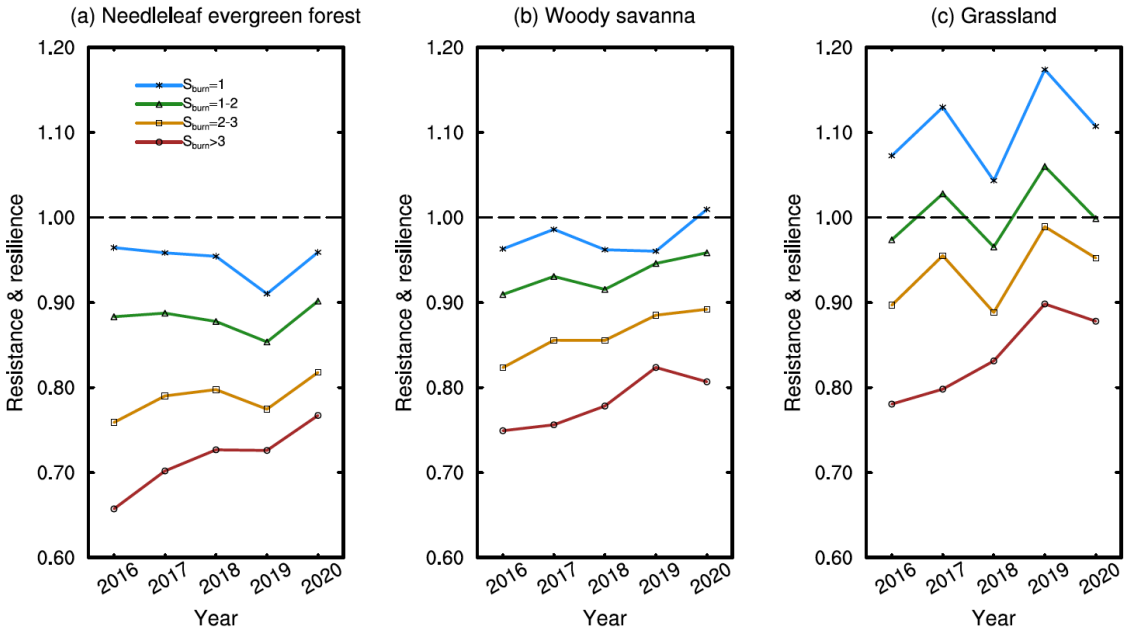

Figure 10. ET characterized temporal trends in fire resistance (2016) and resilience (2017–2020) for (a) needleleaf evergreen, (b) woody savanna, and (c) grassland with four burn severity categories.

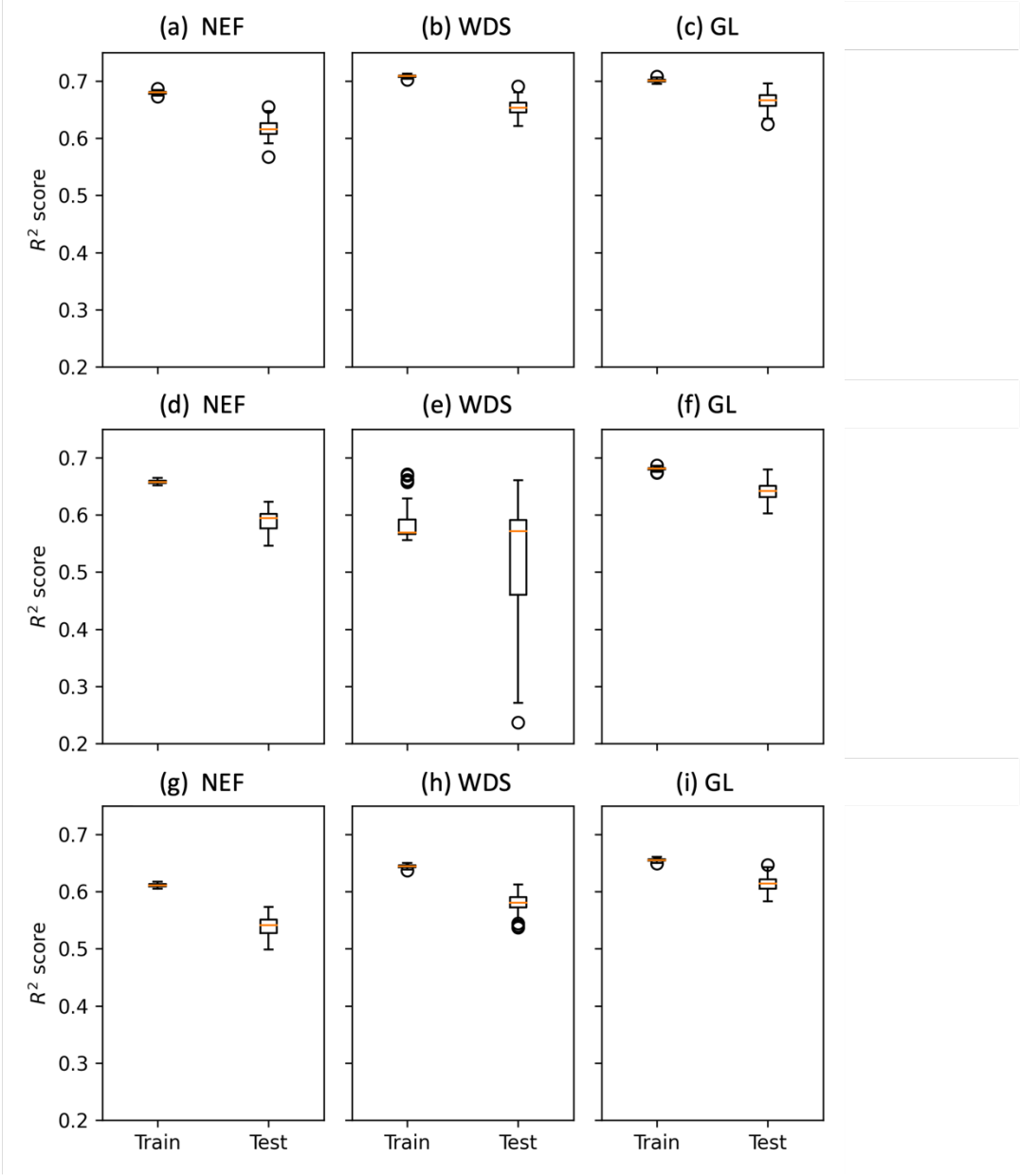

Figure S11. The R^2 scores for the random forest model on train and test datasets for the (a) needleleaf evergreen forest (NEF), (b) woody savanna (WDS), and (c) grassland (GL) VTs represented by LAI, the (d) NEF, (e) WDS, and (f) GL VTs represented by GPP, and for (g) NEF, (h) WDS, and (i) GL VTs represented by ET.

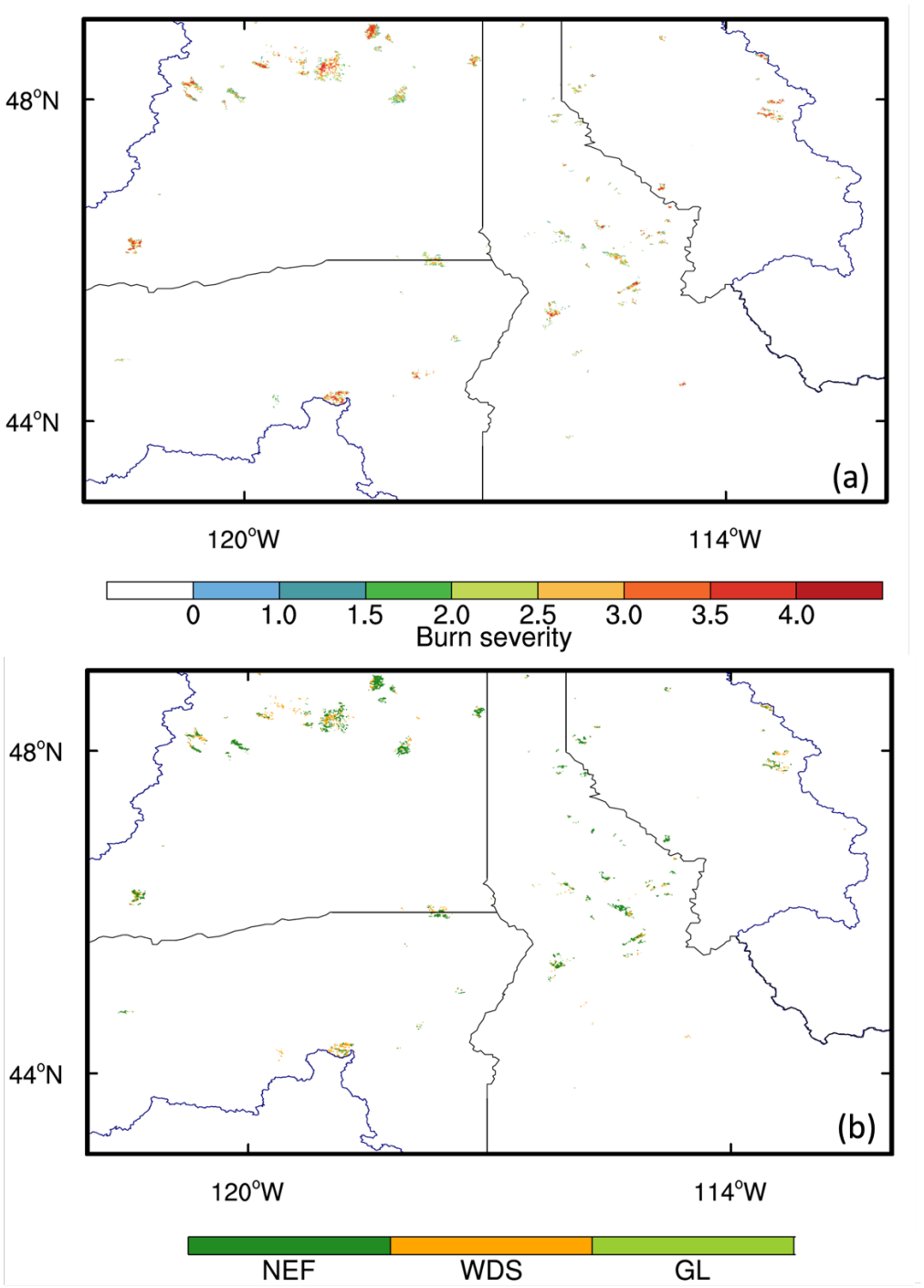

Figure S12. The spatial distribution of (a) the burn severity of data pixels experienced the 2015 fires and (b) the pre-fire (i.e., 2014) VTs in the corresponding pixels of (a). NEF, WDS, and GL represent needleleaf evergreen forest, woody savanna, and grassland, respectively. This figure is similar to Figure 5 with a smaller area and increased image size.

Tables

Table S1. The data products used in this research.

Data variables	Spatial resolution	Temporal resolution	Data time spans	Analysis time spans	Data sources	Reference
Precipitation	30 km	Monthly	1940–ps.	2010–2020	ERA5	Hersbach et al. (2020)
Surface air temperature	30 km	Monthly	1940–ps.	2010–2020	ERA5	Hersbach et al. (2020)
Vapor pressure deficit	30 km	Monthly	1940–ps.	2010–2020	ERA5	Hersbach et al. (2020)
Burn severity	30 m	Annual & event	1984–ps.	2015	MTBS	Eidenshink et al. (2007)
Vegetation type	500 m	Annual	2002–ps.	2015	MODIS	Sulla-Menashe et al. (2018)
LAI	500 m	4-day	2002–ps.	2010–2020	MODIS	Myneni et al. (2002)
GPP	1000 m	8-day	2002–ps.	2010–2020	MODIS	Running et al. (2004)
ET	1000 m	8-day	2002–ps.	2010–2020	MODIS	Mu et al. (2007)

Table S2. The Monitoring Trends in Burn Severity (MTBS) data product indicated burn severity categories at the 30-meter (i.e., original) and the 500-meter (i.e., upscaled) spatial resolutions.

Burn severity categories	At the 30-meter spatial resolution	At the 500-meter spatial resolution
Unburned to low	1	1
Low	2	1–2
Moderate	3	2–3
High	4	>=3

Table S3. The pre- and post-fire precipitation (P; mm $year^{-1}$) and surface air temperature (T_s; °C) in three vegetation types (VTs) in the Columbia River Basin. This calculation does not separate data pixels with different burn severity, but averages the P and Ts data pixels with the same VTs across all the fire boundaries. Here, NEF=Needleleaf evergreen forest, WDS=woody savanna, and GL= grassland.

	NEF		WDS		GL	
	P	T_s	P	T_s	P	T_s
$Mean_{11–14}$	1086.9±125.2	5.1±0.6	1011.5±116.2	4.8±0.6	803.2±103.3	6.6±0.6
$Mean_{16–20}$	1051.5±96.8	5.3±0.5	984.1±83.4	5.1±0.5	797.4±63.3	6.8±0.5

Reference:

Mu, Q., Heinsch, F. A., Zhao, M., and Running, S. W.: Development of a global evapotranspiration algorithm based on MODIS and global meteorology data, *Remote Sensing of Environment*, 111(4), 519-536, [data set], https://doi.org/10.1016/j.rse.2007.04.015, https://modis.gsfc.nasa.gov/data/dataprod/mod16.php, 2007.